EFDA TASK TWO-T429/01: Titanium Alloys Irradiation Testing
(Extension)

The effect of hydrogen on the fracture toughness of the titanium alloys Ti6Al4V and Ti5Al2.5Sn before and after neutron irradiation

Centre de Recherche en Physique des Plasmas,
Technologie de la fusion
Association Euratom- Confédération Suisse
Ecole Polytechnique fédérale de Lausanne
5232 Villigen , PSI, Switzerland

prepared by Pierre Marmy

Contributors:

Maria Luppo *
Ferenc Hegedues ++
Martin Brütsch ●
Zlatko Kopajtic ●
Marlene Krois ●
Pierre Marmy

* On leave, Commission atomique argentine, Buenos Aires
++ X-ray consulting, CH-5232 Villigen
• Paul Scherrer Institut, CH-5232 Villigen

Summary:

1. Introduction.

The ITER first wall modules are attached to the vacuum vessel by a set of four radial flexibles cartridges. Due to their excellent elasticity and strength properties, titanium alloys have been proposed as materials for fabricating the supports. Among a set of proposed alloys, the European home team is checking the properties of two candidate alloys, the alpha+beta Ti6Al4V and the alpha phase Ti5Al2.5Sn alloy. In a previous task BL14.2, the tensile, fatigue and fracture toughness properties have been studied before and after irradiation (see references[1-4]). Although the study is still underway for extending the irradiation temperature window (ITER tasks TW1-TVV), it appears that in the particular dose and temperature range of ITER at the flexibles (0.1 dpa, T_{irr}= 100 to 250°C), the use of both alloys seems to be possible, from the point of view of the irradiation resistance.
In ITER, the titanium parts will not only be exposed to neutron irradiation but also to a partial pressure of hydrogen from the plasma environment. Titanium alloys have a high affinity to hydrogen and therefore can retain it. At a certain hydrogen concentration , hydrides can precipitate and alter the mechanical properties. Under the ITER condition, it is difficult to assess how much hydrogen would enter the titanium. It seems that only two mechanisms are available : by diffusion through the surface oxide layers or by transmutation reaction from the high energy neutrons. The first mechanism should not contribute much because the temperature is relatively low at the flexibles. The second mechanism will yield some hydrogen production. From the neutronics calculation done under the ITER neutron spectrum [5] an hydrogen production of 0.5 appm is expected (Helium will also be generated and will alter the properties. But this is not the object of the present task. The helium production at the flexibles is only 0.15 appm). Hydrogen is not expected to be a big concern for the titanium parts in ITER. Nevertheless, since hydrogen solubility increases with decreasing temperature, even very low hydrogen concentrations can create problems in components having large temperature gradients.
The aim of the present task is to investigate the effect of hydrogen on the fracture toughness properties of the alloys presented above, before and after the irradiation with neutrons. For the purpose of loading hydrogen in known quantities, an hydrogen loading equipment has been developed. The specimen used in the study is the mini-charpy DIN 50115 KLST with dimensions 4x3x27 mm. Because of the small size of the specimen chosen and the activity problems, a special three point bend fracture toughness fixture was also designed and manufactured.
As stated in the ITER task TWO-T429/01, the effect of the neutron irradiation on the fracture toughness properties should be studied at a dose of 0.3 dpa and at a temperature of 50 °C and 350°C.

2. Origin, structure and chemical analysis of the alloys.

The Ti5Al2.4Sn alloy was provided by the SIBER HEGNER & CO. AG, Zürich . The origin of the material is the HOWMET Mill, USA. The material obeys the AMS 4926H specification. After hot forming, it has been annealed 1hr at 815°C and then air cooled. The finished stock is round bar of 31.75 mm. The microstructure consists of equiaxed grains of 20 μm. The chemical specification is given below.

The Ti6Al4V alloy was bought at Firth-Stahl AG, Dübendorf and comes from the TIMET, Savoie SA in UGINE, France. It was produced according to the specification WL 3.7164.1 and DIN 65040/65174 to a stock diameter of 150mm. After hot forming in the alpha + beta field, it has been annealed for 1.5 hr at 730 °C and then air cooled The structure consists of equiaxed alpha grains of about 20 μm , containing secondary alpha zones surrounded by beta phase.

The specimens were cut in the longitudinal direction of the rods, in the L-R or L-C orientation.

Table 1: Chemical compositions: [wt %]

	Al	C	Fe	Sn
Ti5Al2.4Sn	5.0	0.17	0.36	2.4
Ti6Al4V	6.08	0.0056	0.1399	-

H_2	N_2	O_2	V	Others
0.0036	0.010	0.179	-	
<0.0060	0.0065	0.176	3.95	<0.4

3. Microstructure of the as received alloys.

The microstructure of the as received alloys has been investigated and described in details in the previous ITER task BL14 [3, 6]. Below a summarized description is given as a refresher.

Ti5Al2.5Sn

The Ti5Al2.5Sn alloy has a globular appearance with grains mostly of the order of 20 μm. Some larger grains of about 40 μm or more also exist. Usually the larger grains contain smaller ones . A precipitation of an iron riched phased has been detected in the grains , both by optical and transmission microscopy. The TiFe precipitates have a size around 100nm and are located at the grain boundaries and inside the grains. They are generated due to the high iron concentration in the alloy (0.36 wt%). No hydrides are present in the *as received* microstructure.

Ti6Al4V

The Ti6Al4V alloy has a globular structure, composed by primary alpha grains around 20 μm in size and colonies of secondary elongated α grains, surrounded by intergranular β phase. The fraction volume of the β phase is around 13 %. Due to its different composition the β phase is quite visible at the boundaries and appears as intergranular bands of 0.05 to 1 μm width. Some small quantities of residual martensite can be observed in the larger β grains. No hydrides are observed.

4. Hydrogen Charging

Accepted hydrogen limits

According to a large amount of results collected in the scientific literature, a level below 150 wppm H (<0.015wt%) is considered as safe and will not affect the slow strain rate tensile properties of pure titanium and α and α+β titanium alloys. Under very low strain rates (creep regime), some special embrittlement mechanisms can take place and have detrimental effects even at very low hydrogen levels. Some beta alloys (containing no Al) have safe limits up to 250 wppm H. These limits are commonly accepted in the technical literature (Titanium, Metals Handbook, Ninth Edition, Volume 3) and by most titanium producers. The limit below which the fracture toughness and high strain rate properties (Charpy) are not affected by hydrogen, is not well established and will be test parameter and alloy dependent.
The limit of 150 wppm H has been adopted by most manufacturers as the maximum H concentration acceptable in their titanium products.

Hydrides formation

The phase relationships in the titanium-hydrogen system are very complex and H pressure dependent [7]. The impurities in commercial titanium are of sufficient quantity to cause large deviations from the binary Ti-H behaviour [8]. Especially the presence of large quantities of Al in both alloys (5 and 6%) is causing a large increase of the eutectoid temperature for the beta phase and an unknown increase of the terminal solubility limit for the hydride precipitation in the alpha phase [9]. This situation is depicted in a schematic way in Figure 1 according to references [8, 9]. In the frame of this study, assuming H concentrations are below 2000 wppm, and considering that the microstructure of the Ti6Al4V alloy consists mainly of alpha phase, only the following phase reaction will be of interest:

α Ti +H = γ Hydride

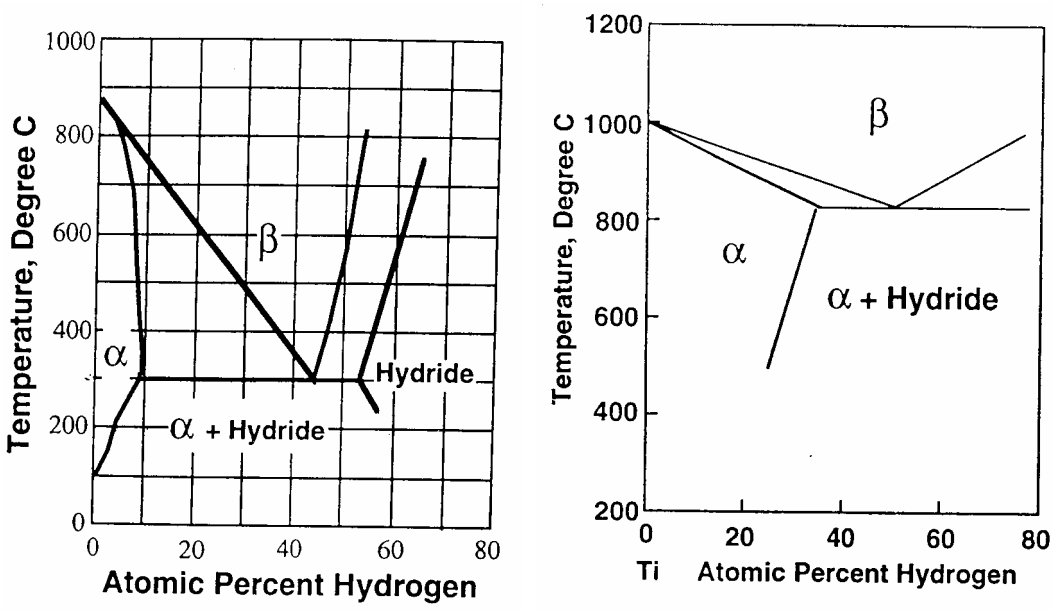

Figure 1: Schematic representation of the Ti-H phase diagram for pure Ti (left) and with approximately 6% Aluminium (right)

Hydrides precipitation in Ti-6Al-4V and Ti5Al-2.5Sn alloys

Hydride precipitation in Ti-6Al-4V was found to depend strongly upon both microstructure and hydrogen content as follows [10, 11]:

- In equiaxed alpha + beta material (alpha grains size: 2-5 μm and beta grains size: 0.5-1 μm) γ-hydride precipitation begins at > 200 ppm and occurs preferentially at alpha/beta interfaces. This is approximately the microstructure of the Ti6Al4V of this study (see[3]).
- In fully transformed beta material γ-hydride precipitation begins at ~ 800 ppm and two new types of hydride are present at ~ 1200 ppm.
- In primary alpha + transformed beta microstructures (~45% equiaxed primary alpha plus 55% transformed beta) γ-hydride begin to be precipitated at ~ 1100 ppm at the primary alpha/transformed beta interfaces.

Hydrides precipitation in the near alpha Ti-5Al-2.5Sn occurs at > 300 ppm as needles of γ-hydride upon $\{10\text{-}10\}_\alpha$ planes [12]:

- Hydride precipitation depends of the cooling rate. In air cooled Ti-5Al-2.5Sn specimens, the precipitates formed throughout the material with no apparent preference for particular nucleation sites and the individual precipitates were frequently of a length comparable to the grain size. However, slowly cooled specimens containing similar amounts of hydrogen exhibited very fine-scale, heterogeneously nucleated precipitates which lay predominantly in the grain boundaries and formed an almost complete network around them [13].

Hydrogen loading charges

A precipitation of hydrides is not expected in both alloys below the 200 wppm limit (0.02 wt%). Therefore the effect of hydrogen without hydrides is investigated at a H charge of **150 wppm**

The effect of hydrogen with precipitated hydrides is investigated at a H charge of **400 wppm**, at which a precipitation of hydrides is expected in both alloys.

4.1 Hydrogen Charging Equipment

Hydrogen absorption by titanium alloys is usually performed in a Sieverts' apparatus [14]. A Sieverts' apparatus consists in a quartz tube, where are introduced the samples to be charged, one end closed and the other end connected, by means of valves, to a vacuum and a gas input systems, where it is possible to measure pressures and temperatures (Figure 2).

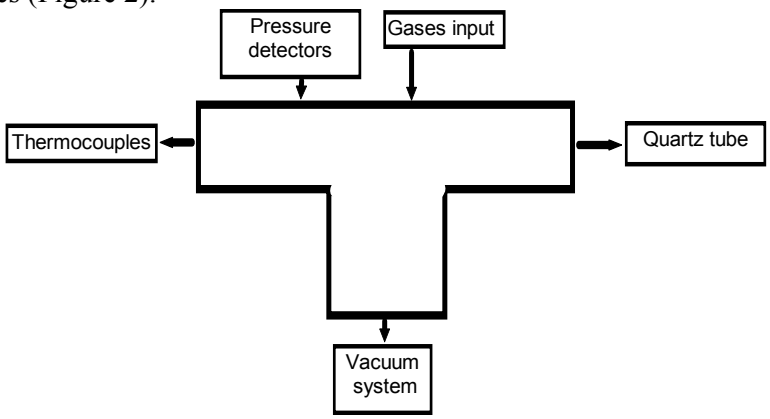

Figure 2: Sketch of the Sieverts's apparatus

The hydrogenation equipment shown in Figure 3, was designed and constructed in the Lab PPH 972, CRPP, EPFL, according to the scheme shown above [15].

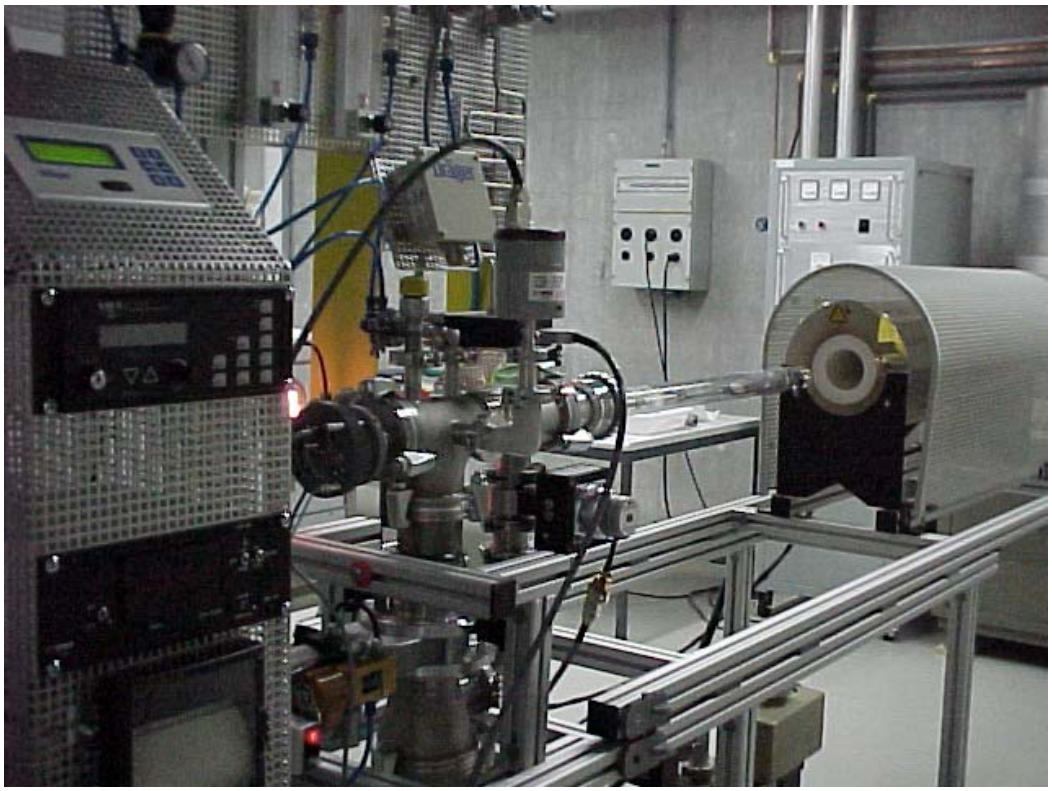

Figure 3: Hydrogenation equipment designed and constructed in the Lab PPH 972, CRPP, EPFL.

The following points must be considered in selecting the conditions for the hydrogen charging:

1. Surface oxides must be completely dissolved. Since surface barriers become less effective at elevated temperatures, hydrogen can be rapidly absorbed and can penetrate deeply into a titanium structure. The natural oxide film on titanium begins to break down at temperatures above about 650°C, hence temperatures below 700°C, at least for initial absorption, are risky. The hydrogenation temperatures found in the literature from titanium are between 650 and 850°C for Ti-6Al-4V [16, 17].
2. If the surface is dirty or has a lot of gases absorbed before the hydrogen sorption, the sample will not absorb hydrogen until those gases or contaminant layers are removed. Then, before each sorption experiment the sample must be degassed by heating at 750°C and 10^{-6} mbar for several minutes to reduce the impurities in the body of the samples increasing the free available volume to be occupied by hydrogen atoms and to activate the surface for hydrogenation [18].
3. The initial absorption time is not thickness dependent, but the achievement of a uniform hydrogen distribution depends on diffusion, and diffusion times are roughly proportional to the square of the thickness for a given temperature and inversely proportional to hydrogen diffusion coefficient ($t = x^2/D$). Hirohata et al

[19] measured the diffusion coefficient of Ti-6Al-4V alloy at constant temperatures (700, 750, 800 and 830°C) and obtained

$$D_{Ti-6Al-4V} = 6.6x10^{-3} \exp\left[\frac{-65438}{RT}\right]$$

According of the points mentioned above and analyzing several hydrogen charging datas found in the literature, for example [19], the hydrogen charging was carried out following the next steps:

0. Before to hydrogen charging, the samples are cleaned in acetone, trichlorethylene and propyl alcohol.
1. Samples degassing at 750°C for 1 hour under dynamic vacuum of 4 x 10^{-7} torr.
2. Stabilization of pressure to room temperature.
3. Vacuum system isolation.
4. Injection of hydrogen to the main T-tube.
5. Samples heating in the furnace at 750°C.
6. Sorption of hydrogen.
7. Homogenization of the hydrogen in the specimens inside the furnace during 4 hours.
8. Cooling at room temperature extracting the quartz tube for the furnace, injection of nitrogen to primary pump, injection argon to the equipment to accelerate the cooling, remaining hydrogen and argon scavenging. This process was necessary because leaving the hydrogen in the tube during cooling down, resulted in much higher hydrogen contents because the solubility of hydrogen is greater at lower temperatures.

The hydrogen concentration in the titanium alloys was estimated using the ideal gas equation :

$$p(torr) = 0.03118 \frac{C_H(ppm) m_{Ti}(g) T(K)}{V(cm^3)}$$

where p[torr] is the pressure, C_H[ppm] is the hydrogen concentration, m_{Ti} is the specimens weight, T is the temperature and V[cm^3] is the equipment volume, derived from flow rates measurements. A typical hydrogen pressure versus time diagram is shown in Figure 4 for a specimen charged to 150 wppm H.

In order to check the achieved hydrogen content, 18 specimens of both types have been test loaded with hydrogen and then subsequently measured in a LECO gas detector. In this system, the specimen are vacuum melted and the thermal conductivity of the outgassing hydrogen is measured in a gas analyser. The LECO system has been calibrated with titanium and Zircaloy calibration pellets. The accuracy was shown to be better than 3% [20]. The hydrogen contained in the *as*

received materials was analysed by gas mass spectrometry. The test results are as follows (Table 2):

Table 2: Hydrogen concentration measured in the titanium alloys before and after hydrogenation in wppm. Specimens I14C26 and I25C17 were measured after irradiation and test at 350°C. Mean from three measurements.

	As received	Annealed, 5hrs at 750°C	150 wppm	400 wppm	400 wppm after irradiation and test
Ti5Al2.5Sn	72.1 and 96.5	4.9	152	435	418 I14C26
Ti6Al4V	24.2 and 34.4	4.7	167.3	436	426 I25C17

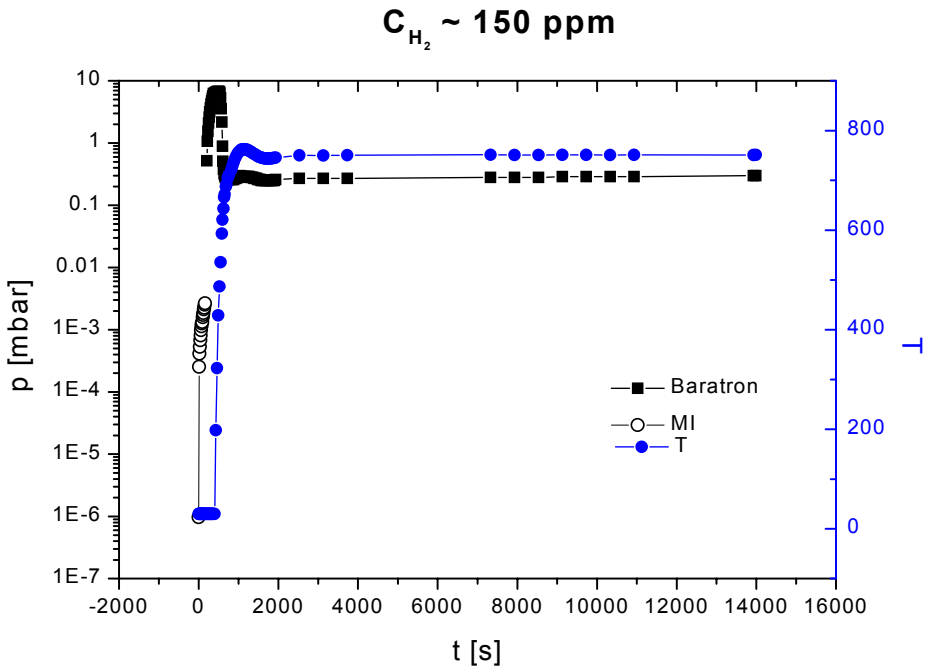

Figure 4. Typical hydrogen pressure and temperature distribution diagram for a specimen charged to 150 wppm

4.2 Specimen Matrix

As shown in the preceding section, a specimen being H charged, is exposed to a complex thermal process in which first the specimen are degassed at high temperature and then subsequently exposed to an hydrogen atmosphere. During the first part of the cycle, the hydrogen content is modified compared with the *as received* material. The alloy receives also *an annealing heat treatment* with some influence on the tensile properties. In order to check the effect, tensile tests have been performed after the heat treatment for both alloys. The alpha alloy was slightly softened by the heat treatment whereas the alpha beta was well resisting. The results of these tests have been shown in the first part of task BL 14 (see report[3]). On the other hand, as shown in Table 2, the hydrogen content in the *as received* material is not negligible for both alloys. Therefore, in order to have a clear comparison, beside the two hydrogen charges of 150 ppm and 400 ppm, the annealed condition has been added in the test matrix. For every condition, four specimen are prepared. Because two irradiation temperature are investigated (50 and 350°C), a total of 48 specimen are necessary to fill the irradiation matrix shown in Table 4. The same number of specimen is contained in the unirradiated comparison matrix shown in Table 5. Some specimen which could not be irradiated in the RISO DR3 reactor for logistical reasons, have been marked with a sign♣. It is planned to irradiate the missing specimens in the BAGIRA Rig of the AEKI reactor in Budapest.

5. Specimen Dosimetry

Unfortunately only scarce information is available on the neutronics of the DR3 reactor at RISO. The core of the DR3 reactor is loaded with highly enriched uranium. The irradiation rig is placed near the core. The neutron spectrum is expected to be very close to an U235 spectrum. For determining the accumulated dose, the neutron flux at the specimen location must be known with precision. In order to solve the problem, the dosimetry results of the similar reactor in Hungary will be used . The 10 MW reactor of the Atomic Research Institute of Budapest (AEKI) is like the DR3, a light water moderated and cooled reactor. Both reactor have a similar power output (10MW) and construction and it can be assumed that their flux will also be similar. Of course, this comparison will only allow a rough assessment of the deposited dose. By means of two dosimetry detector sets, the fast neutron fluence (E>1 MeV) was determined in the BAGIRA loop of the AEKI reactor [21]. Cu, Fe, Ni and Nb detectors have been enclosed in quartz tubes and irradiated together with the specimen. The following reactions have been measured and evaluated according to standard methods [22, 23]:

$^{93}Nb(n,n')^{93m}Nb$
$^{63}Cu(n,\alpha)^{60}Nb$
$^{54}Fe(n,p)^{54}Mn$
$^{58}Nb(n,p)^{58}Co$

Since the threshold energies and the cross sections of the reactions produced are energy dependent, the fast neutron flux calculated from each reaction

are identical only if the neutron spectrum is correct. This was not exactly the case in the first evaluation of the AEKI spectrum, therefore the niobium reaction was chosen as the reference one, because it is less sensitive to spectrum effects. The **dpa** was calculated by using the Greenwood cross section for Ti (averaged with the AEKI spectrum), which is 1451 kbarn and the neutron fluence values of the Nb detectors.

The assessment of the dose accumulated in the DR3 irradiation was done in comparing the activity of identical Ti5Al2.5Sn specimen irradiated in both reactors. This comparison would be strictly valid only if both reactors had the same neutron spectra at the irradiation position, which is obviously not the case:

The ratio of the fast neutron fluences can be estimated from:

$$\frac{\Phi_{Budapest}}{\Phi_{Riso}} = \frac{A_{tn}(Budapest)}{A_{tn}(Riso)} * \frac{Fs(Budapest)}{Fs(Riso)} * \frac{\sigma_{Riso}}{\sigma_{AEKI}}$$

Where A_{tn} is the activity at the end of the irradiation, F_s is the saturation coefficient [24] and σ is the average neutron cross section (E>1.0 MeV) of ^{46}Ti(n,p) ^{46}Sc reaction.

The specimens listed in Table 4 have been irradiated in the RISO reactor in four different batches. The above ratio has been evaluated for several specimens belonging to four different batches [25].

The following results have been obtained [25]:

Irradiation	Fast neutron fluence [cm^{-2}] E>1MeV	dpa
MAKII-10 HT2-A4	$0.631\ 10^{20}$	0.110
12-126 AE HT2-A4	$0.759\ 10^{20}$	0.132
MAKII-11 HT-2-E4	$0.274\ 10^{20}$	0.048
MAKIII-3 HT-3-E4	$0.303\ 10^{20}$	0.053

Table 3: Fast neutron fluence and displacements per atom after the irradiations in DR3

Material	T_{irr} = 60°C	T_{irr} = 350°C
Ti-5Al-2.4Sn (annealed)	14C13 ❶	14C9 ❷
	14C14	14C10 ❷
	14C15	14C11 ❶
	14C16	14C12
Ti-5Al-2.4Sn (C_H = 150 ppm)	14C17 ❶	14C21 ❶ LD
	14C18 ❶	14C22 ❷ LD
	14C19	14C23 LD
	14C20	14C24 LD
Ti-5Al-2.4Sn (C_H = 400 ppm)	14C29♣	14C25 ❶ LD
	14C30♣	14C26 ❷LD
	14C31♣	14C27 LD
		14C28 LD
Ti-6Al-4V (annealed)	25C5	25C1 ❷
	25C6 ❶	25C2 ❶
	25C7 ❷	25C3
	25C8	25C4
Ti-6Al-4V (C_H = 150 ppm)	25C9	25C13 ❷ LD
	25C10 ❶	25C14 ❶ LD
	25C11	25C15 LD
	25C16♣	25C12 LD
Ti-6Al-4V (C_H = 400 ppm)	25C21 VTT	25C17❷ LD
	25C22 VTT	25C18❶ LD
	25C23 VTT	25C19 LD
	25C24♣	25C20 LD

Table 4: Irradiation matrix. ♣ specimen missing to be irradiated in Bagira, ❶ specimen tested with J1C at 22°C, ❷ specimen tested with J1C at 350°C , **LD** specimens which received a dose of 0.05 dpa

Material	T_{test} = 22°C	T_{test} = 350°C
Ti-5Al-2.4Sn (annealed)	14C1 ❶	14C5 ❷
	14C6	14C2 ②
	14C3	14C7
	14C4	14C8
Ti-5Al-2.4Sn (C_H = 150 ppm)	14C33	14C37 ②
	14C34	14C33 ❷
	14C35 ❶	14C39
	14C36	14C40
Ti-5Al-2.4Sn (C_H = 400 ppm)	14C45 ❶	14C41②
	14C46	14C42 ❷
	14C43	14C47
	14C44	14C48
Ti-6Al-4V (annealed)	25C25 ❶	25C29
	25C30	25C26 ②
	25C27	25C31
	25C32	25C28 ❷
Ti-6Al-4V (C_H = 150 ppm)	25C33 ❶	25C37
	25C38	25C34 ②
	25C39	25C35 ❷
	25C36	25C40
Ti-6Al-4V (C_H = 400 ppm)	25C41	25C45 ❷
	25C46	25C42 ②
	25C43	25C47
	25C44 ❶	25C48

Table 5: Unirradiated comparison matrix.❶❷= J1C tested at 22, 350°C ①② = BCT (Blow Crack Toughness) tested at 22, 350°C

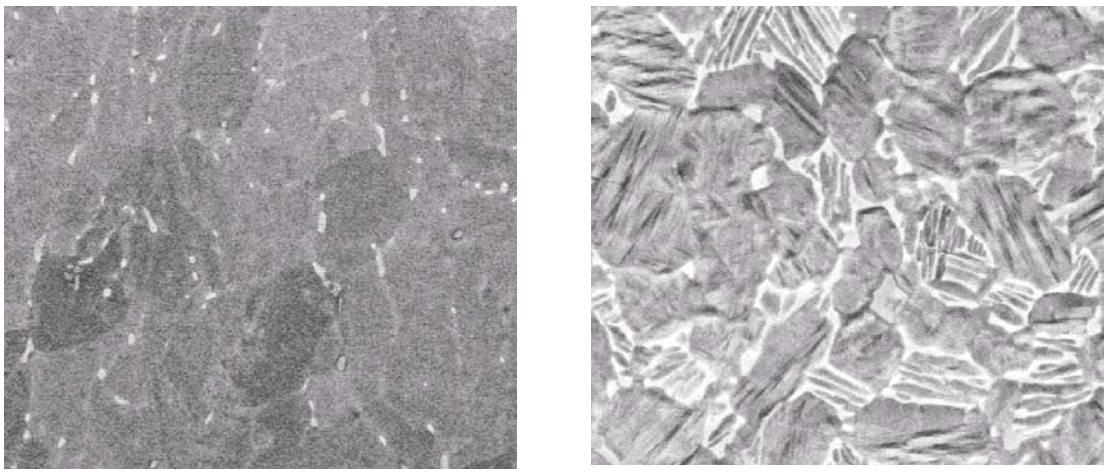

Figure 5: SEM micrographs showing a) the structure of the annealed Ti5Al2.5Sn, globular α grains decorated with residual β phase (white dots) b) the structure of the annealed Ti6Al4V alloy, globular α grains, transformed acicular α phase and intergranular β phase (white).

6.0 Metallurgical examination after hydrogenation and irradiation

Miscroscopic examination of polished surfaces of both alloys has been carried out, in order to eventually reveal the formation of hydrides. The specimens were observed in the scanning electron microscope Zeiss DSM 962. The appearance of the micrographs was dependant on the hydrogen content, but no hydrides could be observed. Fig 5 shows the microstructure for both alloys, after the hydrogenation heat treatment but without hydrogen. Fig 6 presents the influence of hydrogen on phase morphology in the α+β alloy. Fig 6a shows the annealed structure without hydrogen. The grain interior reveals a fine lamellar structure. The grains are surrounded by the β phase which appears as a white contrast. Fig 6b and c show the structure after 150 wppm and 400 wppm H loaded. The hydrogen has removed the inner structure but the surronding β phase does not seem to have changed significantly. Fig 7 shows the influence of increasing levels of hydrogen on the structure of the α alloy. The residual β phase which appears as white dots, seems to become coarser but the interior of the grains shows increased surface distorsion and the formation of micro-cracks at grain boundaries (Fig 7c and Fig 8). The appearance of the micrographs was generally not changed by the irradiation. The structure revealed by SEM was very similar after irradiation for all conditions, except for α+β alloy irradiated at 350°C. This is shown in Fig 9 which compares the structure irradiated at 60°C and the structure irradiated at 350°C. The high temperature structure shows less contrast in the grain interior and deep erosion at the location of the β phase.

The specimens were then etched with an etchant of following composition : 10 ml HF, 25 ml HNO3, 45 ml glycerol and 20 ml water. The specimens were observed in a Jenaphot 2000 optical microscope. The etching did not reveal any hydrides.
The results of the micrographic analysis indicate clearly that hydrogen promotes

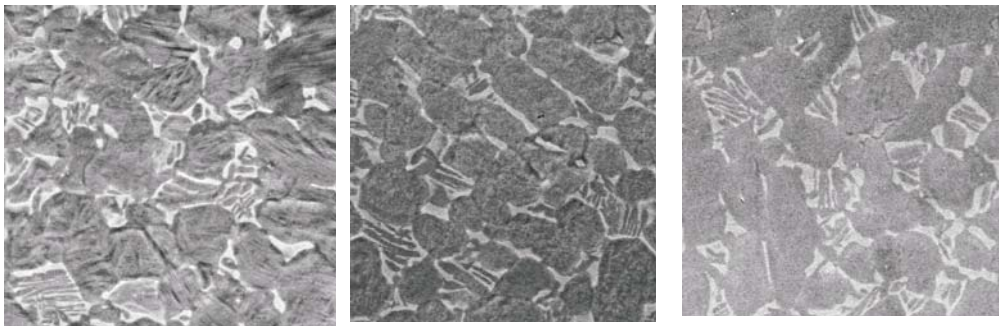

Figure 6: Influence of hydrogen content on the structure of the Ti6Al4V alloy: a) no hydrogen b) 150 ppm c) 400 ppm. SEM micrographs

structural changes in both alloys. Based on the SEM information only, it is not possible to describe the induced changes. Skotnikova et al.[26] have described the structural modifications which result from hydrogenation annealing and hydrogen loading into a near alpha alloy. Of course, the alloys in this study are more stable compositions, nevertheless the modifications observed by SEM in the morphology of the grain interiors reveal structural modifications induced by hydrogen and its

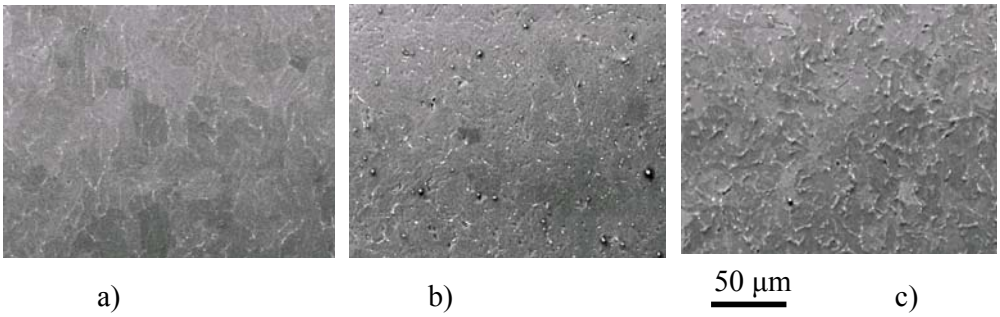

Figure 7: Influence of hydrogen content on the structure of the Ti5Al2.5Sn alloy: a) no hydrogen b) 150 ppm c) 400 ppm. SEM micrographs

β–stabilizing effect. The morphological changes shown in Fig. 6 are similar to those reported by Kohn et al [27] and [10] in the case of hydrogen-treated Ti6Al4V alloy. In the α alloy, using surface microscopy, it was not possible to reveal the presence of hydrides, even at 400 ppm H. Although the hydrogen level is higher than the solubility limit of the α phase, the residual β phase present in the alloy may have absorbed the excessive hydrogen. The residual β phase is a consequence of the high Fe concentration (Table 1) [2]. Nevertheless hydrides may be present in the microstructure of both alloys, occupying a low volumetric fraction. Only a detailed study by transmission electron microscopy could have clarified this point.

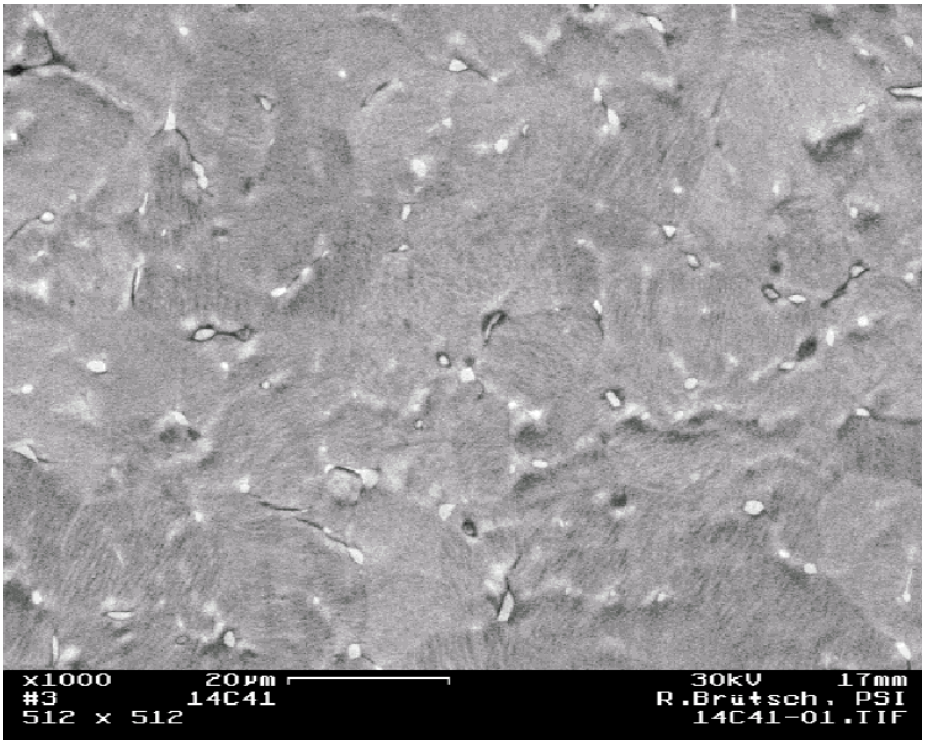

Figure 8: Some micro-cracks along the grain boundaries in Ti5Al2.5Sn loaded with 400ppm H

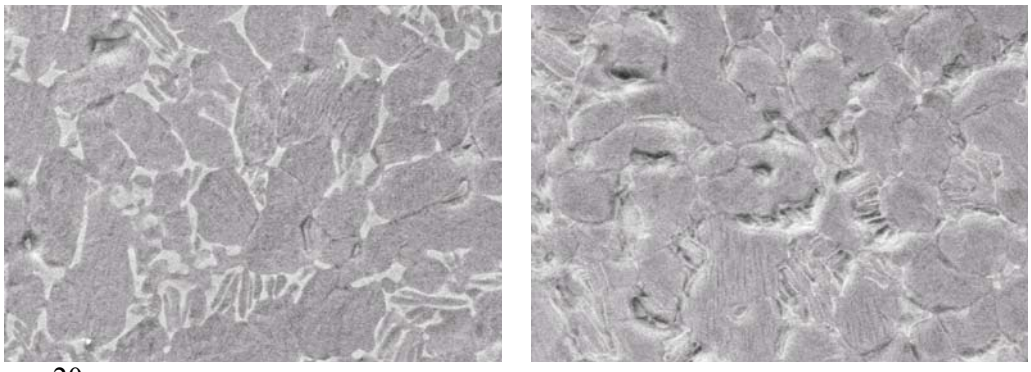

Figure 9: The effect of irradiation on the structure of the Ti6Al4V alloy a)T_{irr}=60°C/0.13 dpa b) T_{irr}=350°C/0.11 dpa. SEM micrographs. No hydrogen.

7.0 Fracture toughness test description

The fracture toughness is best described in titanium alloys using the concept of J_{IC} [4]. The J_{IC} value is the limit where the material starts to resist to the crack extension. This method is best suitable for materials in which crack growth is slow and stable. The test is accomplished according to ASTM standards E813 or E1737 (new version). The specimen recommended is a bend specimen with a deep sharp pre-crack. The specimen selected for this study is a mini-charpy DIN 50115 KLST (see Figure 10). A special fixture has been specially developed to fit the small size of the specimen and to be capable of very simple handling as requested by the radioactivity of the specimen. The specimen can be deposited with tweezers in a self centering support (see Figure 11). The fixture is placed in the grips of an RMC100 -INSTRON testing machine. The test is run under vacuum at a pressure near 10^{-6} mbar. As requested in the norm a crack having a length of .5 to .75 times the width, needs to be introduced in the specimen before testing. The crack is grown on site in the already irradiated specimen, by doing a fatigue pre-test. The specimens were cut in the longitudinal direction of the rods, in the L-R or L-C orientation.
The test consists of measuring the J-R curve, which is a plot of the J-integral versus the physical crack length. The specimens were deformed at a constant rate of 0.5 mm/min. The property J_{IC} is extracted from the J-R curve according to the procedure described in the norm E813.

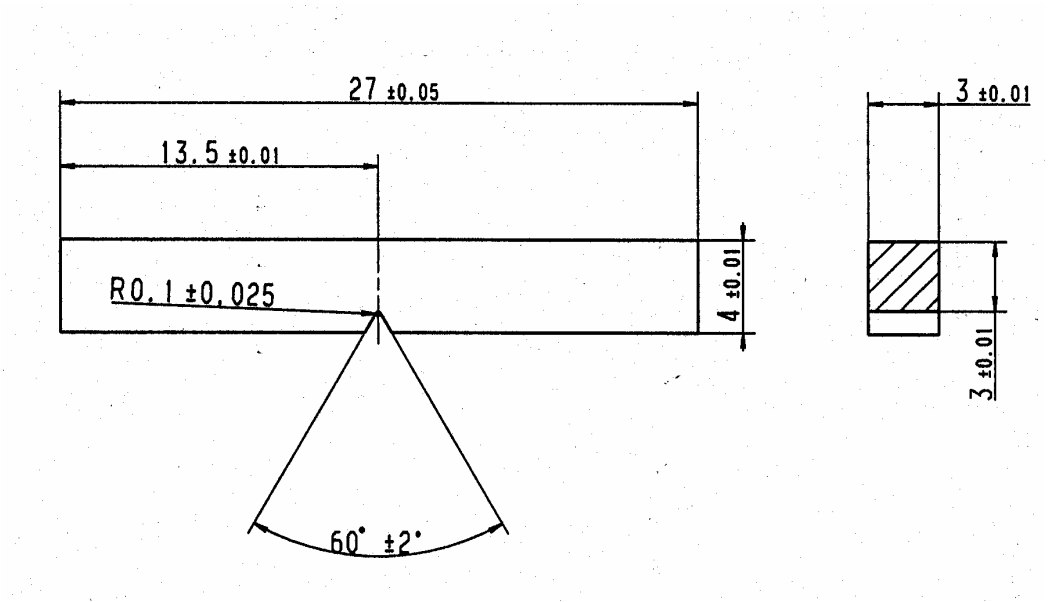

Figure 10. Mini-charpy DIN 50115 KLST

The measurement of the length of the crack is done using two different methods.

- The compliance methods measures the apparent elasticity of the specimen. The effective crack length is then calculated using the compliance transfer relation of Jablonski[28]. An example of the Load versus Center displacement is shown in Fig. 12 for a typical 3-point bend Ti5Al2.5Sn specimen.
- The electrical potential drop over the crack is measured with spun contacts placed below the specimen. The crack length is then deduced from a calibration curve. The measurement is done using a MATELECT device and the results directly transferred to the INSTRON testing electronic. In order to eliminate the thermal effects, a dummy specimen is also measured in line with the tested specimen (see Figure 11).

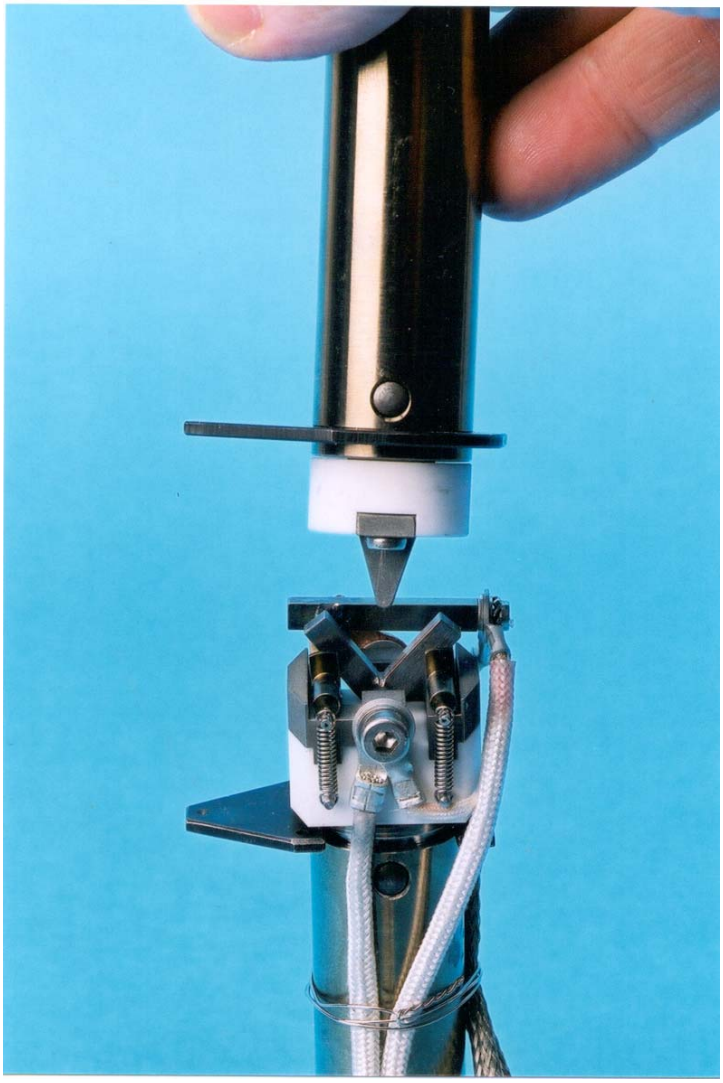

Figure 11. View of the mini 3-point bend test fixture.

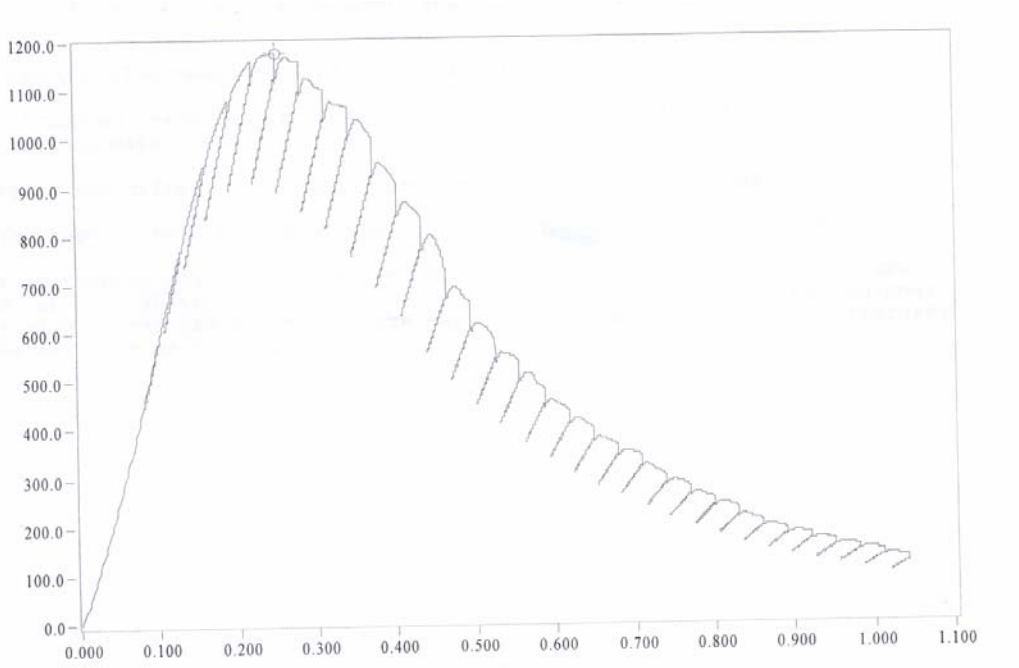

Figure 12: Typical load (N) displacement (mm) diagram for a Ti5Al2.5Sn specimen

7.1 Fracture Toughness tests results

The values obtained for the crack initiation fracture toughness are shown in Table 6 for the Ti5Al2.5Sn alloy and in Table 7 for the Ti6Al4V alloy. The influence of initial condition, hydrogen content and irradiation temperature on J_Q at a test temperature of 22°C, is shown in Fig 13 for the α+β alloy and Fig 14, for the α alloy. In the *as received* condition, both alloys show initiation fracture toughness values J_Q around 60 kJ/m^2. After the hydrogenation annealing heat treatment (data points labeled as *unirradiated* in Figs 13 to 16), J_Q value is increased to 115 kJ/m^2 for the α alloy and to 120 kJ/m^2 for the α+β alloy. For the α alloy Ti5Al2.5Sn, the values obtained in the condition annealed and irradiated are significantly larger than in the *as received* condition. In the contrary, the values measured in the α+β alloy are reduced by a factor more than three after irradiation at 60°C (J_Q = 15 kJ/m^2) and 350°C (J_Q = 23 kJ/m^2), to nearly 0.12 dpa.

In the unirradiated case and for the α alloy, J_Q decreases linearly as a function of the hydrogen level, whereas for the α+β alloy, a sharp decrease of J_Q occurs at 150 ppm H followed by slight recovery at 400 ppm H. The condition irradiated and hydrogen loaded is dramatic for both alloys. The measured value for J_Q was generally between 10 and 20 kJ/m^2. The only exception was the Ti5Al2.5Sn alloy irradiated at 350°C to 0.05 dpa, which indicated at 150 ppm H, a J_Q value of 40 kJ/m^2. The influence of initial condition, hydrogen content and irradiation temperature on J_Q at a test temperature of 350°C, is shown in Fig 15 for the α+β alloy and Fig 16, for the α alloy. In the *as received* condition, the Ti6Al4V alloy showed a very high initiation

fracture toughness, which in fact resulted from extensive crack blunting and absence of crack propagation (Fig 13). At a test temperature of 350°C, and for both alloys, the J_Q values were only weakly influenced by the hydrogen level. The J_Q values were slightly higher in the α alloy as compared to the α+β alloy. The same lack of hydrogen content dependence was also observed in the irradiated material, for both alloys. Nevertheless the value was much lower in the α+β alloy (J_Q around 40 kJ/m^2) as compared to the α alloy (J_Q = 95 kJ/m^2). All hydrogen-loaded specimens irradiated at 350°C, whose values are reported in Figs. 5and 6, received a dose of 0.05 dpa. To check for the thermal stability of the irradiation structure, a specimen irradiated at 60°C was tested at 350°C. It indicated a J_Q of 50 kJ/m^2, a value quite low as compared to the unirradiated case but considerably higher as compared to the result obtained at room temperature (15 kJ/m^2). Brittle rupture of specimens in the test fixture did not occur for any specimen. Even at very low J_Q values, stable crack growth prevailed.

Table 6:
Fracture Toughness Properties of Titanium Ti5Al2.5Sn

(Units:Mpa,%,°C,%/min,dpa,kJ/m^2)

Specimen used: DIN 50115 KLST, Width 3 mm, Height 4mm, Length 27mm

Spec. Name	Condition	Irradiation Temperature	Dose	Test Temperature	J_Q
N14C1	annealed	unirradiated	N/A	22	114.4
N14C5	annealed	unirradiated	N/A	350	152
I14C9	annealed	350	0.11	350	86.5
I14C10	annealed	350	0.11	350	98
I14C11	annealed	350	0.11	22	84.7
I14C13	annealed	60	0.132	22	68.7
I14C17	150 ppmH	60	0.132	20	11.8
I14C18	150 ppmH	60	0.132	20	17
I14C21	150 ppmH	350	0.053	22	40.4
I14C22	150 ppmH	350	0.048	350	107
I14C25	400 ppmH	350	0.053	20	16.4
I14C26	400 ppmH	350	0.053	350	82.5
N14C33	150 ppmH	unirradiated	N/A	350	149
N14C35	150 ppmH	unirradiated	N/A	22	91.2
N14C42	400 ppmH	unirradiated	N/A	350	138
N14C45	400 ppmH	unirradiated	N/A	22	38.2
N14C86	as received	unirradiated	N/A	350	130
N14C92	as received	unirradiated	N/A	22	56.6

Table 7:
Fracture Toughness Properties of Titanium Ti6Al4V

(Units:Mpa,%,°C,%/min,dpa,kJ/m^2)

Specimen used: DIN 50115 KLST, Width 3 mm, Height 4mm, Length 27mm

Spec. Name	Condition	Irradiation Temperature	Dose	Test Temperature	J_Q	Remark
I25C1	annealed	350	0.11	350	32.6	
I25C2	annealed	350	0.11	22	22.1	
I25C6	annealed	60	0.132	20	15	
I25C7	annealed	60	0.132	350	47	
I25C10	150 ppmH	60	0.132	20	12.1	
I25C13	150 ppmH	350	0.048	350	38.3	
I25C14	150 ppmH	350	0.048	22	11.8	
I25C17	400 ppmH	350	0.053	350	37.7	
I25C18	400 ppmH	350	0.053	22	13.6	
N25C25	annealed	unirradiated	N/A	22	120	
N25C28	annealed	unirradiated	N/A	350	122.5	
N25C33	150 ppmH	unirradiated	N/A	22	41	
N25C35	150 ppmH	unirradiated	N/A	350	143	
N25C45	400 ppmH	unirradiated	N/A	350	115	
N25C44	400 ppmH	unirradiated	N/A	22	58.4	
N25C77	as received	unirradiated	N/A	22	50.2	
N25C80	as received	unirradiated	N/A	22	63	
N25C89	as received	unirradiated	N/A	22	58.7	
N25C96	as received	unirradiated	N/A	22	67.8	
N25C105	as received	unirradiated	N/A	350	260	no propagation

Tensile tests with and without the annealing for 5hrs at 750°C (heat treatment used to load hydrogen in titanium), have shown in a previous work [1] that the α+β alloy is more stable than the α alloy. The α alloy Ti5Al2.5Sn responded to the treatment by exhibiting reduced strength and enhanced ductility. Fig 13 to 16 indicate nevertheless that both alloys have after the heat treatment, much higher initiation fracture toughness values. This effect is probably the result of the low hydrogen content after the annealing (see Table 2) and of the recovery of the dislocation structure. An exception is shown in Fig 15 for the Ti6Al4V specimen tested at 350°C. At that particular temperature, the *as received* material has a very high uniform elongation [1] which induces extensive crack blunting and prevents the propagation of the crack.

The fracture toughness values obtained in the *as received* condition are consistent with those already published [4]. In the annealed condition, the effect of the irradiation is dramatic for the α+β alloy, even when irradiated at 350°C. It is known

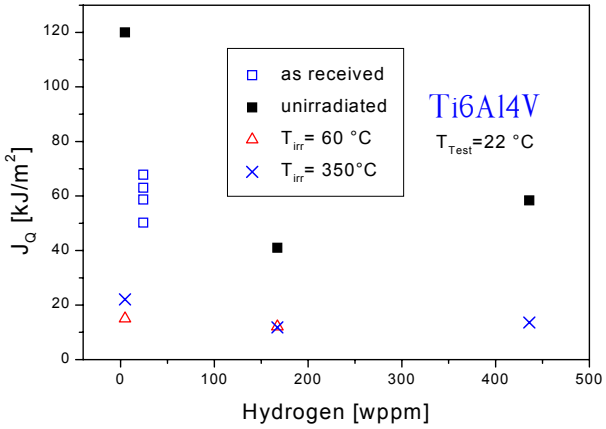

Figure 13: Crack initiation fracture toughness J_Q as a function of the hydrogen content for Ti6Al4V tested at 22 °C

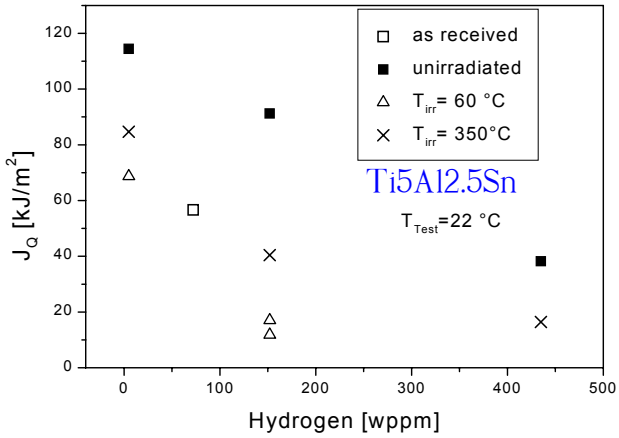

Figure 14: Crack initiation fracture toughness J_Q as a function of the hydrogen content for Ti5Al2.5Sn tested at 22 °C

from previous work, that when irradiated at 350°C, the irradiation induces vanadium rich precipitates and thus induces tremendous hardening and loss of ductility [2, 4]. The behaviour of the unloaded α alloy is much better, may be due to its much simpler structure with less interfaces.

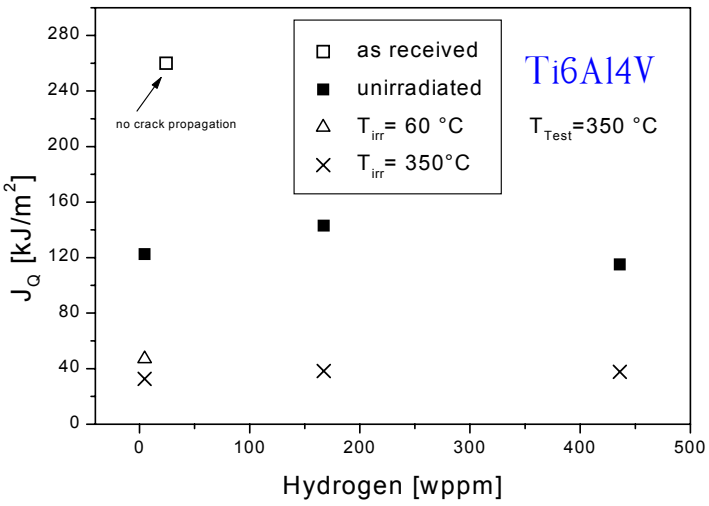

Figure 15: Crack initiation fracture toughness J_Q as a function of the hydrogen content for Ti6Al4V tested at 350 °C

If tested at room temperature, both alloys show a strong dependence of J_Q as a function of hydrogen content, whereas when tested at high temperature, they show only little dependence. The absence of hydrogen content dependence at high temperature could be the combined result of hydrogen in solution as well as in the

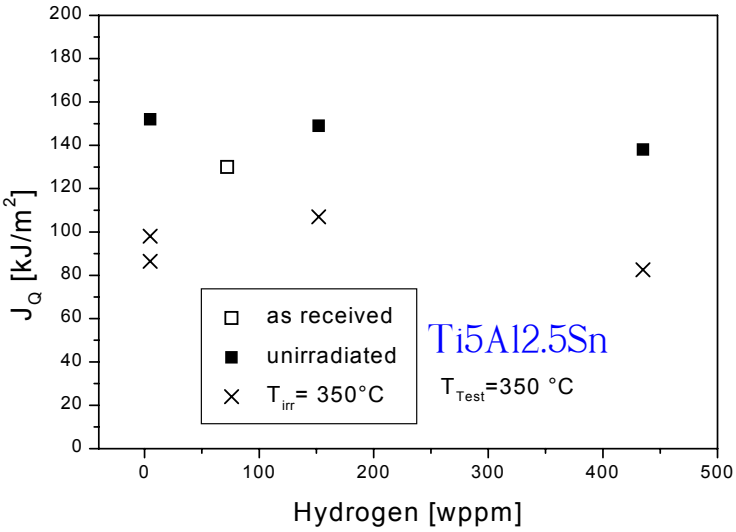

Figure 16: Crack initiation fracture toughness J_Q as a function of the hydrogen content for Ti5Al2.5Sn tested at 350 °C

form of hydrides. The general effect of the irradiation on the hydrogen loaded specimens was to decrease the measured fracture toughness. At T_{irr}=350°C in

Ti5Al2.5Sn, the J_Q value remains larger than 80 kJ/m^2, up to 400 ppm H, but for the other conditions and for both materials, they were reduced by factors between 3 and 5. It is important to note that after the irradiation and the test at 350°C, no hydrogen is escaping the specimen. The hydrogen remaining in the irradiated material after the complete test procedure has been measured to be the same as before the irradiation (see Table 2).
There was no such synergetic effect as reported by Kozhevnikov in α alloys irradiated at 350°C [29], that the irradiation would have reduced the embrittlement by hydrogen. This is probably caused by the high impurity level in our α alloy, so that the dissolved hydrogen cannot be absorbed at the irradiation defects. In the contrary, both damage sources seem to be additive in the present study.
Despite its lower theoretical solubility limit for hydrogen, the Ti5Al2.5Sn alloy has shown a better resistance to hydrogen embrittlement as compared to the Ti6Al4V alloy. This is probably due to the particular microstructures and impurity levels characterizing these two alloys.

8. Conclusions

Specimens of Ti6Al4V and Ti5Al2.5Sn alloys have been loaded with 150 and 400 wppm hydrogen and irradiated with neutrons to a dose between 0.05 and 0.13 dpa, at 60 and 350°C.

- The introduction of hydrogen resulted into structural changes in both materials, as indicated by the SEM micrographic analysis.
- When tested at room temperature, the crack initiation fracture toughness values J_Q decrease as the hydrogen content increases. Tested at 350°C, both alloys show no dependence upon hydrogen content.
- In the irradiated annealed condition and with no hydrogen, the J_Q values are significantly higher in the α alloy Ti5Al2.5Sn as compared with the Ti6Al4V α+β alloy.
- When irradiated and tested at 350°C, the Ti5Al2.5Sn alloy maintains fairly high values of J_Q, up to 400 wppm H.
- In the irradiated hydrogen-loaded condition and when tested at room temperature, both alloys showed low J_Q values, nevertheless brittle failure in the test fixture never occurred.

Acknowledgements:

The Paul Scherrer Institute at Villigen, PSI is sincerely thanked for its logistical and technical support throughout this project. We wish to express our thanks to Brian Oliver from Battelle Memorial Institute for the gas spectrometry analysis.

.

REFERENCES:

1. Marmy, P., et al., *Tensile and Fatigue Properties of two Titanium Alloys as Candidate Materials for Fusion Reactors.* Journal of Nuclear Materials, 2000. **283-287**: p. 602-606.
2. Marmy, P. and T. Leguey, *Impact of irradiation on the tensile and fatigue properties of two titanium alloys.* Journal of Nuclear Materials, 2001. **296**: p. 155-164.
3. Marmy, P., et al., *The tensile and fatigue behaviour of the titanium alloys Ti6al4V and Ti5Al2.5Sn before and after irrdiation with protons to doses up to 0.3 dpa*. 2001, CRPP-EPFL: Lausanne. p. 1-46.
4. Tähtinen, S., et al., *Tensile and fracture toughness properties of unirradiated and neutron irardiated titanium alloys.* Journal of Nuclear Materials, 2002.
5. Khripunov, V. and H. Linda, *Damage in Materials of the Separable First Wall and Blanket Attachment Assemblies*. 2000: Garching.
6. Leguey, T., et al., *Microstructure of Ti5Al2.5Sn and Ti6Al4V deformed in tensile and fatigue tests.* Journal of Nuclear Materials, 2002. **305**: p. 52-59.
7. O.Kubaschewski, et al., *Titanium: Physico-Chemical Properties of its Compounds and Alloys*, ed. A.E. Review. Vol. Special Issue No.9. 1983: International Atomic Energy Agency, Wagramerstrasse 5, P.O. Box 100, A-1400 Vienna, Austria. 460.
8. Lewkowicz, I., *Titanium-Hydrogen*, in *Hydrogen Metal Systems I*, F.A. Lewis and A. Aladjem, Editors. 1996, SCITEC Publications Balaban Publishers. p. 239-279.
9. Nelson, H.G., *Hydrogen Effects in Materials*, ed. A.W. Thompson and N.R. Moody. 1996: TMS.
10. Hoeg, H., B. Hollund, and I.W. Hall, *Effect of hydrogen on teh fracture properties and microstructure of Ti-6Al-4V.* Metal Science, 1980: p. 50-56.
11. Hall, I.W., *Hydride Precipitation in Ti-6Al-4V*. Scandinavian Journal of Metallurgy, 1978. **7**: p. 277-281.
12. Hall, I.W., *Hydrides Precipitation in Ti-5Al-2.5Sn.* Scandinavian Journal of Metallurgy, 1978. **7**: p. 187-190.
13. Lenning, G.A., C.M. Craighead, and R.I. Jaffee, *Hydrogen Precipitations in Ti5Al2.5Sn.* Trans. AIME, 1954. **200**: p. 100.
14. McQuillan, A.D., Journal Inst. Met., 1951. **79**: p. 371.
15. Luppo, M., *Hydrogen Charging Equipment Sievert's type*. 1999, CRPP: Villligen.
16. Senkov, O.N. and J.J. Jonas, Met. Mat. Trans. A, 1996. **27A**: p. 1869.
17. Mahayan, Y., S. Nadiv, and W.R. Kerr, Scr. Met., 1979. **13**: p. 695.
18. Waisman, J.L., G. Sines, and L.B. Robinson, Metall. Trans., 1973. **4**: p. 291.
19. Hirohata, Y., et al., Fusion Tech., 1996: p. 363.
20. Krois, M. and Z. Kopajtic, *Bestimmung von Wasserstoff in Titan Proben*. 1999+2003.
21. Hegedues, F., *Titanium alloy specimen irradiation in the AEKI Reactor fast neutron fluence measurement*. 2001, X-Ray Consulting: Villigen.
22. *Test Method for Measuring Fast-Neutron Reaction Rates by Radioactivation of Niobium*, ed. A.S. E1297.

23. *Fast-Neutron Fluence Determination with Niobium Activation Detectors*, ed. D.N. 25456-4.
24. Holzgrewe, F., F. Hegedues, and J.M. Paratte, *Calculation and benchmarking of an azimuthal pressure vessel neutron fluence distribution using the boxer code and scraping experiments.* Nuclear Technology, 1995. **109**: p. 383-397.
25. Hegedüs, F., *Titanium alloy specimen irradiation in the RISO reactor fast neutron fluence measurement*. 2001, X-ray Consulting: Villigen-PSI.
26. Skotnikova, M.A., et al., *Effect of hydrogen on the structure and properties of pseudo-alpha-titanium alloy.* Materials Science and Heat Treatment, 1993. **35**(12): p. 677-681.
27. Kohn, D.H. and P. Ducheyne, *Tensile and fatigue strength of hydrogen-treated Ti-6Al-4V alloy.* Journal of Materials Science, 1991. **26**: p. 328-334.
28. Jablonski, D.A., et al., *Compliance Functions for Various Fracture Mechanics Specimens.* Engineering Fracture Mechanics, 1985. **Vol. 22**(No 5): p. 819-827.
29. Kozhevnikov, O.A., et al., *Neutron irradiation influence on hydride generation and distribution mechanism in titanium alpha alloys.* Physics of Material Damage and Radiation Material Science, 1979. **1-9**(Nuclear Science and Technique Problems): p. 71-74.